Multicritical behavior of the ferromagnetic Blume-Emery-Griffiths model with repulsive biquadratic couplings

A. Ercule* and M. N. Tamashiro†

Instituto de Física "Gleb Wataghin", Universidade Estadual de Campinas, UNICAMP, Rua Sérgio Buarque de Holanda, 777, Cidade Universitária, Campinas, São Paulo, 13083-859, Brazil

(Received 21 February 2018; published 25 June 2018)

The ferromagnetic ($J > 0$) version of the Blume-Emery-Griffiths model in the region of repulsive biquadratic couplings ($K < 0$) is considered on a Cayley tree of coordination z, reducing the statistical problem to the analysis of a two-dimensional nonlinear discrete map. In order to investigate the effect of the coordination z on the system multicritical behavior, we study the particular case $K/J = -3.5$ with the inclusion of crystal fields ($D \neq 0$), but vanishing external magnetic fields ($H = 0$), for two distinct lattice coordinations ($z = 4$ and $z = 6$). The thermodynamic solutions on the Bethe lattice (the central region of a large Cayley tree) are associated with the attractors of the two-dimensional map. The phase diagrams display several thermodynamic phases (paramagnetic, ferromagnetic, ferrimagnetic, and staggered quadrupolar). In some cases, there are regions of numerical costability of two different attractors of the map, associated with discontinuous phase transitions between the corresponding phases. To verify the thermodynamic stability of the phases and to locate the first-order boundaries, the analytical expression of the Gibbs free energy was obtained by the method proposed by Gujrati [Phys. Rev. Lett. **74**, 809 (1995)]. For lower coordinations ($z = 4$) the transition between the ferrimagnetic and the staggered quadrupolar phases is always continuous, while the transition between the ferromagnetic and the ferrimagnetic phases is discontinuous at low temperatures, turning into continuous for temperatures above a tricritical point. On the other hand, for higher coordinations ($z = 6$), the transition between the ferromagnetic and the ferrimagnetic phases is always continuous. However, the transition between the ferrimagnetic and the staggered quadrupolar phases is continuous for higher temperatures and discontinuous for temperatures below a tricritical point, in agreement with previous results obtained in the mean-field approximation (infinity-coordination limit). In both cases, the occurrence and the thermodynamic stability of the ferrimagnetic phase is confirmed.

DOI: 10.1103/PhysRevE.97.062145

I. INTRODUCTION

A generalization of the standard spin-1/2 ferromagnetic Ising model [1] is given by the spin-1 Blume-Emery-Griffiths (BEG) model [2], defined by the Hamiltonian

$$\mathscr{H} = -J \sum_{(\mu,\nu)} s_\mu s_\nu - K \sum_{(\mu,\nu)} s_\mu^2 s_\nu^2 + D \sum_\nu s_\nu^2,$$
$$s_\nu = -1, 0, +1, \tag{1}$$

which includes bilinear J and biquadratic K nearest-neighbor (μ,ν) pair interactions and a single-ion anisotropy term, associated with the local crystal field D at site ν. This model presents a rich variety of critical and multicritical phenomena and can be used to describe spin systems, although originally it was introduced to describe the phase separation and superfluidity in ^{3}He-^{4}He mixtures [2].

Extensions of the BEG model have also been proposed to describe simple [3] and binary [4] fluids, ternary mixtures [5–7], semiconductor alloys [8], microemulsions [9], Langmuir lipid monolayers [10], liquid water [11], etc. Several complementary techniques have been used to investigate the BEG model and its extensions: the mean-field approximation (MFA) [2–10,12–15], the Bethe-lattice (BL) or Bethe-Peierls approximation (BPA) [11,16–22], renormalization-group (RG) theory [12,23–25], Monte-Carlo renormalization-group (MCRG) theory [26], cluster variation method (CVM) [27] and Monte Carlo simulations (MCSs) [20,25,28–30]. The majority of these analyses predict interesting features of the phase diagrams of the BEG-like models.

In particular, the ferromagnetic ($J > 0$) version of the BEG model with repulsive biquadratic couplings ($K < 0$) yields under the MFA [12–14] extremely rich phase diagrams, exhibiting reentrant behavior, terminal critical points, multicritical points, and the occurrence of four distinct thermodynamic phases: paramagnetic (P), ferromagnetic (F), staggered quadrupolar (SQ), and ferrimagnetic (Fi). On the other hand, the RG calculations [12,24,25], which go beyond the MFA, predict that the Fi phase squeezed between the F and SQ phases is present in three dimensions, but does not survive to thermal fluctuations in two dimensions. The MCRG [26] confirms the results for $K/J = -1.5$ by MFA and RG in three dimensions. The CVM [27] predicts, for the cubic lattice and $K/J = -3$, a transition between two distinct ferrimagnetic phases. The MCSs predict the absence of the Fi phase even in three dimensions [20,28], as well as in two dimensions [25,29]. Nevertheless, some previous results obtained on the BL for $K/J = -3.5$, but without a thermodynamic analysis

*aercule@ifi.unicamp.br
†mtamash@ifi.unicamp.br

based on a consistent free energy [21], suggest that, for lower coordinations, the transition between the Fi and the SQ phases is always continuous, while the transition between the Fi and the F phases is discontinuous for lower temperatures and continuous for higher temperatures. For higher coordinations, in agreement with the MFA results [12–14], the transition between the Fi and the F phases is always continuous, while the transition between the Fi and the SQ phases is discontinuous for lower temperatures and continuous for higher temperatures. Whenever the phase boundary changes character, this is related to the existence of a tricritical point.

We believe thus that it is still possible to explore the effect of the lattice coordination z on the multicritical behavior of the BEG ferromagnetic model with repulsive biquadratic couplings. We were in part motivated by the need to check the robustness of the MFA predictions and to locate the first-order phase boundaries inside the regions of numerical costability, associated with the overlapping regions of stability of two distinct attractors on the BL. Since an expression for the consistent Gibbs free energy on the BL has not been found in previous works, it was not possible to establish the thermodynamic phase of the system in these costability regions. Therefore, in order to complete the previous results found on the BL [21,22], we obtain the thermodynamically consistent BL Gibbs free energy by using the method proposed by Gujrati [31].

The layout of this paper is as follows. In Sec. II we formulate the spin-1 BEG model on a Cayley tree of coordination z and obtain the nonlinear recursion relations. Their attractors correspond to the solutions on the BL, deep in the interior of a large tree [32,33]. We study the effect of the lattice coordination z on the multicritical behavior of the ferromagnetic model ($J > 0$) and the inclusion of a crystal field D in the region of repulsive biquadratic couplings, in the particular case $K/J = -3.5$. First we analyze the numerical stability of the map attractors in Sec. III. For the range of parameters investigated, this BEG model displays uniform and alternate (staggered) phases, forcing us to split the tree into two interpenetrating sublattices. In Sec. IV we obtain the Gibbs free-energy density per site by Gujrati's method [31], for both the uniform and the staggered cases. By collecting results from the previous sections for two typical values of coordination of the Cayley tree, $z = 4$ and $z = 6$, we construct in Sec. V global $T \times D$ phase diagrams, including the first-order phase boundaries. Finally, some concluding remarks are presented in Sec. VI.

II. BEG MODEL ON A CAYLEY TREE

The Cayley tree is a connected graph without closed loops, as illustrated in Fig. 1 by five successive generations of a tree with coordination $z = 3$. The calculations for the standard Ising model on the Cayley tree and their physical interpretation on the BL are well established [32–36]. The statistical problem can be formulated in terms of a nonlinear discrete map, whose attractors correspond to the physical solutions in the interior of a tree far removed from its surface, the so-called BL [32,33]. These solutions are expected to provide approximations for the BEG model on a regular lattice with the same coordination z, generally identical to the traditional BPA [37–40].

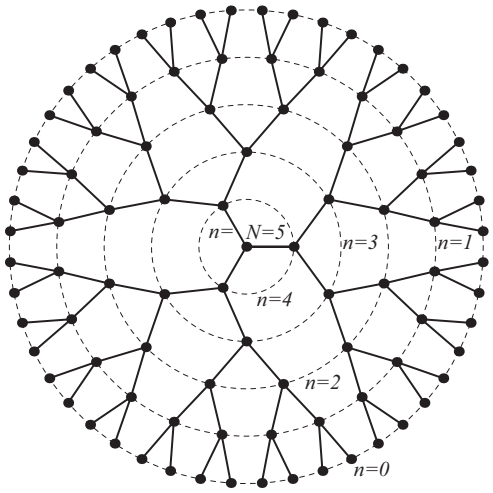

FIG. 1. Cayley tree with coordination number $z = 3$ and $N = 5$ generations of sites. The generations are labeled from the surface ($n = 0$) to the central site ($n = N = 5$).

The BEG model [2] on a Cayley tree of N generations is defined by the Hamiltonian

$$\mathscr{H}_N = -J \sum_{(\mu,\nu)} s_\mu s_\nu - K \sum_{(\mu,\nu)} s_\mu^2 s_\nu^2 + D \sum_\nu s_\nu^2 - H \sum_\nu s_\nu,$$
$$s_\nu = -1, 0, +1, \tag{2}$$

where the (μ,ν) sums extend over all nearest-neighbor pairs of sites of a Cayley tree of coordination z and the ν sums are over all single sites. Notice that, in order to bypass the constraint of fixed magnetization $M \equiv \sum_\nu s_\nu$ in the (semi)canonical ensemble, the Gibbs magnetic ensemble will be used, so that a Zeeman contribution associated with an external magnetic field H was added to the BEG Hamiltonian Eq. (1). Furthermore, the inclusion of the magnetic field H and the crystal field D single-site terms allows one to readily obtain the equations of state for the thermal averages $\langle s_\nu \rangle$ and $\langle s_\nu^2 \rangle$ by free-energy differentiation. At the end of the calculations, one may set $H = 0$.

Let us consider the BEG model formulated on a Cayley tree of N generations, with the central site located at the generation $n = N$, as depicted in Fig. 1. The partition function of the complete tree in the Gibbs magnetic ensemble is given by

$$Y_N = \sum_{\{s_\nu\}} e^{-\beta \mathscr{H}_N} = \sum_{\{s_\nu\}} \exp\left(j \sum_{(\mu,\nu)} s_\mu s_\nu + k \sum_{(\mu,\nu)} s_\mu^2 s_\nu^2 - d \sum_\nu s_\nu^2 + h \sum_\nu s_\nu \right), \tag{3}$$

where the trace $\{s_\nu\}$ represents a sum over all possible spin microstates, $\beta = (k_B T)^{-1}$, k_B is the Boltzmann constant, T is the absolute temperature, and we introduce the dimensionless parameters $j \equiv \beta J$, $k \equiv \beta K$, $d \equiv \beta D$, and $h \equiv \beta H$.

It is convenient to define the partial partition functions of the whole tree $Y_N^{(s)}$, obtained with a fixed central spin s ($s = -1, 0, +1$),

$$Y_N = \sum_s Y_N^{(s)}. \tag{4}$$

Note that each $Y_N^{(s)}$ depends on the partial partition functions of the z tree branches connected to the central spin s. Thus we can write

$$Y_N^{(s)} = e^{-ds^2+hs}\left[\sum_{\sigma=0,\pm1} e^{j\sigma s+k\sigma^2 s^2} Q_{N-1}^{(\sigma)}\right]^z, \tag{5}$$

where $Q_n^{(\sigma)}$ is the partial partition function of a tree branch with n layers far from the surface, when the innermost site (root of the branch) at generation n has spin σ. This explicit distinction between the partial partition functions of the entire tree $Y_N^{(\sigma)}$ and of the tree branches $Q_N^{(\sigma)}$ is necessary in order to solve the model iteratively. One can take advantage of the cycle-free structure of the Cayley tree to establish the following recursion relations [32,33] between tree branches of successive generations:

$$Q_{n+1}^{(s)} = e^{-ds^2+hs}\left[\sum_{\sigma=0,\pm1} e^{j\sigma s+k\sigma^2 s^2} Q_n^{(\sigma)}\right]^{z-1}, \tag{6}$$

with the fixed spin s located at generation $n+1$, and the traced spins σ at generation n. Each innermost spin s at the root of a tree branch is connected now to $(z-1)$ outer tree branches, leading thus to a distinct exponent from the previous $Y_N^{(s)}$ formula. For a Cayley tree with N generations, the boundary condition at the tree surface implies

$$Q_0^{(s)} \equiv e^{-ds^2+hs}, \tag{7}$$

because the surface spins (at generation $n=0$) interact only with the spins of the generation $n=1$.

It is convenient now to introduce the ratios

$$x_{n+1} \equiv \frac{Q_{n+1}^{(+)}}{Q_{n+1}^{(0)}} = e^{-d+h}\left(\frac{1+e^{j+k}x_n+e^{-j+k}y_n}{1+x_n+y_n}\right)^{z-1}, \tag{8}$$

$$y_{n+1} \equiv \frac{Q_{n+1}^{(-)}}{Q_{n+1}^{(0)}} = e^{-d-h}\left(\frac{1+e^{-j+k}x_n+e^{j+k}y_n}{1+x_n+y_n}\right)^{z-1}, \tag{9}$$

which define a two-dimensional nonlinear discrete map $(x_n,y_n)\to(x_{n+1},y_{n+1})$.

The physically acceptable solutions far from the tree surface, i.e., on the BL, correspond to attractors of the map problem. In this case, for the range of parameters investigated, the attractors found are either single fixed points, for which $(x,y)=(x_{n+1},y_{n+1})=(x_n,y_n)$,

$$x = e^{-d+h}\left(\frac{1+e^{j+k}x+e^{-j+k}y}{1+x+y}\right)^{z-1}, \tag{10}$$

$$y = e^{-d-h}\left(\frac{1+e^{-j+k}x+e^{j+k}y}{1+x+y}\right)^{z-1}, \tag{11}$$

or two-cycle fixed points (orbits of period two), for which $(x_a,y_a)\to(x_b,y_b)\to(x_a,y_a)$ under the map transformation, where the subscripts a and b label two distinct sublattices. In other words, by using the same previous discrete map, Eqs. (8) and (9), we have $(x_a,y_a)=(x_{n+1}^a,y_{n+1}^a)=(x_{n-1}^a,y_{n-1}^a)$ and $(x_b,y_b)=(x_{n+2}^b,y_{n+2}^b)=(x_n^b,y_n^b)$, with $(x_a,y_a)\neq(x_b,y_b)$. Thus the set (x_a,x_b,y_a,y_b) associated with a two-cycle fixed point satisfies the coupled system of nonlinear equations,

$$x_a = e^{-d_a+h_a}\left(\frac{1+e^{j+k}x_b+e^{-j+k}y_b}{1+x_b+y_b}\right)^{z-1},$$

$$x_b = e^{-d_b+h_b}\left(\frac{1+e^{j+k}x_a+e^{-j+k}y_a}{1+x_a+y_a}\right)^{z-1}, \tag{12}$$

$$y_a = e^{-d_a-h_a}\left(\frac{1+e^{-j+k}x_b+e^{j+k}y_b}{1+x_b+y_b}\right)^{z-1},$$

$$y_b = e^{-d_b-h_b}\left(\frac{1+e^{-j+k}x_a+e^{j+k}y_a}{1+x_a+y_a}\right)^{z-1}. \tag{13}$$

At the end of the calculations, the sublattice-dependent parameters $d_a\equiv\beta D_a$, $d_b\equiv\beta D_b$, $h_a\equiv\beta H_a$, and $h_b\equiv\beta H_b$ will be set to $d_a=d_b=d$ and $h_a=h_b=h=0$. They are introduced here in order to easily carry out thermal averages by free-energy differentiation.

III. MAP ATTRACTORS, BETHE-LATTICE ORDER PARAMETERS, AND BIFURCATION DIAGRAMS

The numerical analysis consists primarily to iterate the discrete map given by Eqs. (8) and (9), looking for stable single fixed points or two-cycle fixed points (orbits of period 2), which are related to the possible thermodynamic phases on the BL. However, since the variables (x_n,y_n) are unbounded, it is convenient to introduce the auxiliary variables

$$\bar{m}_n \equiv \frac{x_n-y_n}{1+x_n+y_n} = \bar{m}_n(\bar{m}_{n-1},\bar{q}_{n-1}), \tag{14}$$

$$\bar{q}_n \equiv \frac{x_n+y_n}{1+x_n+y_n} = \bar{q}_n(\bar{m}_{n-1},\bar{q}_{n-1}), \tag{15}$$

which are limited to the ranges $-1\leqslant\bar{m}_n\leqslant 1$ and $0\leqslant\bar{q}_n\leqslant 1$, simplifying thus the numerical search for attractors. Henceforth, instead of looking for attractors of the recursion relations Eqs. (8) and (9), we will use the fully equivalent forms given by Eqs. (14) and (15).

We have found stable single fixed points, for which $(\bar{m},\bar{q})=(\bar{m}_{n+1},\bar{q}_{n+1})=(\bar{m}_n,\bar{q}_n)$, or stable two-cycle fixed points, for which $(\bar{m}_a,\bar{q}_a)\to(\bar{m}_b,\bar{q}_b)\to(\bar{m}_a,\bar{q}_a)$ under the discrete map (14) and (15). It should be remarked that the stable single fixed point associated with the above auxiliary variables,

$$\bar{m}(x,y) = \lim_{N\to\infty}\frac{\sum_s sQ_N^{(s)}}{\sum_\sigma Q_N^{(\sigma)}} = \frac{x-y}{1+x+y}, \tag{16}$$

$$\bar{q}(x,y) = \lim_{N\to\infty}\frac{\sum_s s^2Q_N^{(s)}}{\sum_\sigma Q_N^{(\sigma)}} = \frac{x+y}{1+x+y}, \tag{17}$$

where (x,y) is a single fixed point satisfying Eqs. (10) and (11), is not related to the thermodynamic order parameters, magnetization $m\equiv\langle s_v\rangle$, and quadrupole moment $q\equiv\langle s_v^2\rangle$, respectively, which must be defined on the BL. These BL order parameters are given by statistical averages in the central region of an infinite Cayley tree, but can be also obtained by partial derivatives of the Gibbs free-energy density Eq. (29),

to be obtained in Sec. IV,

$$m \equiv \langle s_v \rangle = \lim_{N\to\infty} \frac{\sum_s s Y_N^{(s)}}{\sum_\sigma Y_N^{(\sigma)}} = \frac{[1+e^{j+k}(x+y)](x-y)}{1+e^{j+k}(x^2+y^2)+2(e^{-j+k}xy+x+y)} = -\left(\frac{\partial \beta g}{\partial h}\right)_d \neq \bar{m}, \tag{18}$$

$$q \equiv \langle s_v^2 \rangle = \lim_{N\to\infty} \frac{\sum_s s^2 Y_N^{(s)}}{\sum_\sigma Y_N^{(\sigma)}} = \frac{e^{j+k}(x^2+y^2)+2e^{-j+k}xy+x+y}{1+e^{j+k}(x^2+y^2)+2(e^{-j+k}xy+x+y)} = \left(\frac{\partial \beta g}{\partial d}\right)_h \neq \bar{q}. \tag{19}$$

In fact these equations of state represent the traditional BPA [37–40] applied for the BEG model.

For the stable two-cycle fixed points, we define analogously

$$\bar{m}_a \equiv \frac{x_a - y_a}{1+x_a+y_a}, \quad \bar{m}_b \equiv \frac{x_b - y_b}{1+x_b+y_b}, \quad \bar{q}_a \equiv \frac{x_a + y_a}{1+x_a+y_a}, \quad \bar{q}_b \equiv \frac{x_b + y_b}{1+x_b+y_b}, \tag{20}$$

in terms of (x_a, x_b, y_a, y_b) given by Eqs. (12) and (13). Again, the thermodynamic order parameters on the BL can be found by statistical averages in the central region of an infinite Cayley tree or by partial derivatives of the Gibbs free-energy density considering two sublattices, Eq. (30),

$$m_a \equiv \langle s_a \rangle = \frac{e^{j+k}(x_a x_b - y_a y_b) + e^{-j+k}(x_a y_b - x_b y_a) + x_a - y_a}{1+e^{j+k}(x_a x_b + y_a y_b) + e^{-j+k}(x_a y_b + x_b y_a) + x_a + x_b + y_a + y_b} = -2\left(\frac{\partial \beta g}{\partial h_a}\right)_{h_b,d_a,d_b} \neq \bar{m}_a, \tag{21}$$

$$m_b \equiv \langle s_b \rangle = \frac{e^{j+k}(x_a x_b - y_a y_b) - e^{-j+k}(x_a y_b - x_b y_a) + x_b - y_b}{1+e^{j+k}(x_a x_b + y_a y_b) + e^{-j+k}(x_a y_b + x_b y_a) + x_a + x_b + y_a + y_b} = -2\left(\frac{\partial \beta g}{\partial h_b}\right)_{h_a,d_a,d_b} \neq \bar{m}_b, \tag{22}$$

$$q_a \equiv \langle s_a^2 \rangle = \frac{e^{j+k}(x_a x_b + y_a y_b) + e^{-j+k}(x_a y_b + x_b y_a) + x_a + y_a}{1+e^{j+k}(x_a x_b + y_a y_b) + e^{-j+k}(x_a y_b + x_b y_a) + x_a + x_b + y_a + y_b} = 2\left(\frac{\partial \beta g}{\partial d_a}\right)_{h_a,h_b,d_b} \neq \bar{q}_a, \tag{23}$$

$$q_b \equiv \langle s_b^2 \rangle = \frac{e^{j+k}(x_a x_b + y_a y_b) + e^{-j+k}(x_a y_b + x_b y_a) + x_b + y_b}{1+e^{j+k}(x_a x_b + y_a y_b) + e^{-j+k}(x_a y_b + x_b y_a) + x_a + x_b + y_a + y_b} = 2\left(\frac{\partial \beta g}{\partial d_b}\right)_{h_a,h_b,d_a} \neq \bar{q}_b, \tag{24}$$

reducing to Eqs. (18) and (19) by setting $x_a = x_b = x$ and $y_a = y_b = y$, as expected.

The numerical stability of the attractors can be checked by a simple linear-stability analysis [41]. In the case of a single fixed point, this can be performed by finding the eigenvalues Λ_i of the Jacobian matrix associated with the original discrete map, Eqs. (8) and (9),

$$\boldsymbol{J}(x,y) \equiv \left.\frac{\partial(x_{n+1}, y_{n+1})}{\partial(x_n, y_n)}\right|_{(x_n,y_n)=(x,y)} = \begin{pmatrix} \frac{\partial x_{n+1}}{\partial x_n} & \frac{\partial x_{n+1}}{\partial y_n} \\ \frac{\partial y_{n+1}}{\partial x_n} & \frac{\partial y_{n+1}}{\partial y_n} \end{pmatrix}_{(x_n,y_n)=(x,y)}, \tag{25}$$

with the partial derivatives evaluated at the single fixed point (x,y) of interest. If $\Lambda_{1,2} \in \mathbb{R}$, (x,y) is an asymptotically stable fixed point when $|\Lambda_{1,2}| < 1$; otherwise it is unstable, if one or both eigenvalues are outside of this range. For $\Lambda_{1,2} \in \mathbb{C}$, then the eigenvalues are necessarily complex conjugate with the same module. For a two-cycle fixed point, the linear-stability analysis is similarly performed by finding the eigenvalues of the matrix product $\boldsymbol{J}(x_a,y_a)\,\boldsymbol{J}(x_b,y_b)$, evaluated along each fixed point of the orbit.

Our main interest here is to confirm and extend previous results obtained on the BL for the ferromagnetic BEG model with repulsive biquadratic interactions and the inclusion of a crystal field [21], concerning its multicritical behavior. We analyze two different lattice coordinations, $z = 4$ (low coordination) and $z = 6$ (high coordination), keeping constant the ratio $K/J = -3.5$ and by varying the dimensionless temperature $t = (\beta J z)^{-1}$ and the ratio D/Jz. In the investigated range of interaction parameters, one may obtain the following thermodynamic phases at vanishing magnetic field ($H = 0$):

(i) paramagnetic phase (P): $m = m_a = m_b = 0$, $q = q_a = q_b \neq 0$;

(ii) ferromagnetic phase (F): $m = m_a = m_b \neq 0$, $q = q_a = q_b \neq 0$;

(iii) staggered quadrupolar or antiquadrupolar phase (SQ): $m_a = m_b = 0$, $q_a \neq q_b$;

(iv) ferrimagnetic phase (Fi): $m_a \neq m_b$, $q_a \neq q_b$;

which are identified according to the above listed values of the order parameters on the BL.

In order to gain some insight about the possible scenarios, it is instructive to plot bifurcation diagrams, showing the profile of the fixed points $(\bar{m}, \bar{q})$ of the auxiliary variables, for fixed dimensionless temperatures $t = (\beta J z)^{-1}$ and by varying the ratio D/Jz. When costability of different attractors is present, a plot of the absolute value of the largest eigenvalue $|\Lambda_1|$ of the Jacobian matrix is also informative. Figures 2–4 correspond to the case of lower coordination ($z = 4$), while Figs. 5–7 deal with the case of higher coordination ($z = 6$).

A. Lower coordination ($z = 4$)

Figure 2 displays two continuous transitions near the abscissas -2.524 (transition from the F to the Fi phase) and -2.517 (transition from the Fi to the SQ phase), associated with bifurcations in the stable solutions. The SQ phase corresponds to a two-cycle fixed point, but this is only evident in the $\bar{q}$ diagram, since both $(\bar{m}_a, \bar{m}_b)$ have null values in this phase. Figure 3 displays, in addition, an unstable branch,

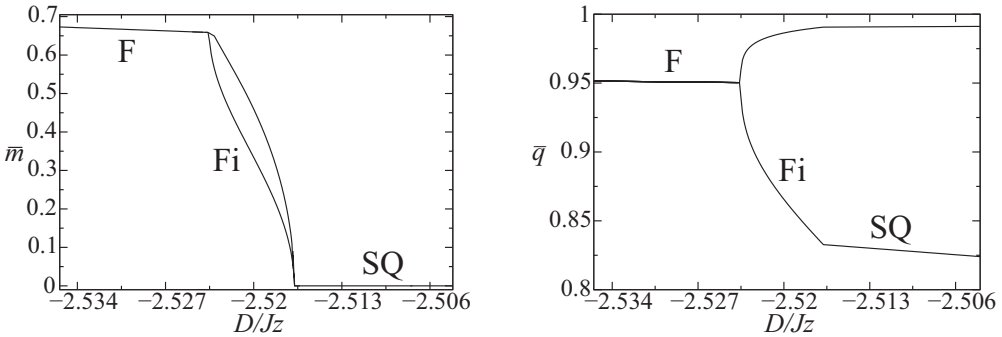

FIG. 2. Bifurcation diagrams of the fixed points $(\bar{m},\bar{q})$ of the auxiliary variables as a function of the parameter D/Jz, with $z = 4$, $K/J = -3.5$, and $t = 0.3$. The thermodynamic phase labels (F, Fi, SQ) follow the main text. For the alternate Fi and SQ phases, the two branches shown correspond to the $(\bar{m}_a,\bar{m}_b,\bar{q}_a,\bar{q}_b)$ values on the two distinct sublattices (a,b).

represented by the dashed lines, which indicates the occurrence of a discontinuous phase transition. In the abscissa range $-2.503 \lessapprox D/Jz \lessapprox -2.501$ it is possible to note in the $\bar{m}$ diagram the numerical costability of the stable branch belonging to the F phase, with $\bar{m}$ about 0.9, and two stable branches (two-cycle fixed point) belonging to a Fi phase, with $(\bar{m}_a,\bar{m}_b)$ less than 0.9. The same features can be observed in the $\bar{q}$ bifurcation diagram.

Due to the onset of this unstable solution, we investigated the eigenvalues of the Jacobian matrix. Figure 4 shows the behavior of the absolute value of the largest eigenvalue $|\Lambda_1|$ in this region. The attractors and repulsors of the mapping are directly connected to the stable and unstable branches of the bifurcation diagrams shown in Fig. 3. The overlap between two numerically costable attractors represents a clear indication of the existence of a discontinuous (first-order) transition between two thermodynamically coexisting (F and Fi) phases. The intersection of $|\Lambda_1|$ values associated with the costable attractors occurs near the point $(-2.503,0.99)$, but cannot be used as a rigorous criterion to discuss the thermodynamical stability of the corresponding phases.

B. Higher coordination ($z = 6$)

Figure 5 displays two continuous transitions near the abscissas -2.56 (transition from the F to the Fi phase) and -2.535 (transition from the Fi to the SQ phase), associated with bifurcations in the stable solutions. The SQ phase corresponds to a two-cycle fixed point, but this is only evident in the $\bar{q}$ diagram, since both $(\bar{m}_a,\bar{m}_b)$ have null values in this phase. Figure 6 displays, in addition, an unstable branch, represented by the dashed lines, which indicates the occurrence of a discontinuous phase transition. In the abscissa range $-2.523 \lessapprox D/Jz \lessapprox -2.493$ it is possible to note in the $\bar{m}$ and $\bar{q}$ diagrams the numerical costability of distinct stable branches, a two-cycle fixed point belonging to a Fi phase, with $(\bar{m}_a,\bar{m}_b)$ above 0.7, and another two-cycle fixed point belonging to the SQ phase with $\bar{m}_a = \bar{m}_b = 0$. In order to improve visualization, the $\bar{q}$ diagram was rescaled by taking the modulus of the decimal logarithm of the difference $1 - \bar{q}$, showing how the stable branches belonging to the Fi and the SQ phases are connected through unstable branches.

Again, motivated by the onset of this unstable solution, we investigated the eigenvalues of the Jacobian matrix. Figure 7 shows the behavior of the absolute value of the largest eigenvalue $|\Lambda_1|$ in this region. The attractors and repulsors of the mapping are directly connected to the stable and unstable branches of the bifurcation diagrams shown in Fig. 6. The overlap between two numerically costable attractors represents a clear indication of the existence of a discontinuous (first-order) transition between two thermodynamically coexisting (Fi and SQ) phases. The intersection of $|\Lambda_1|$ values associated with the costable attractors occurs near the point $(-2.5,0.8)$, but again cannot be used as a rigorous criterion

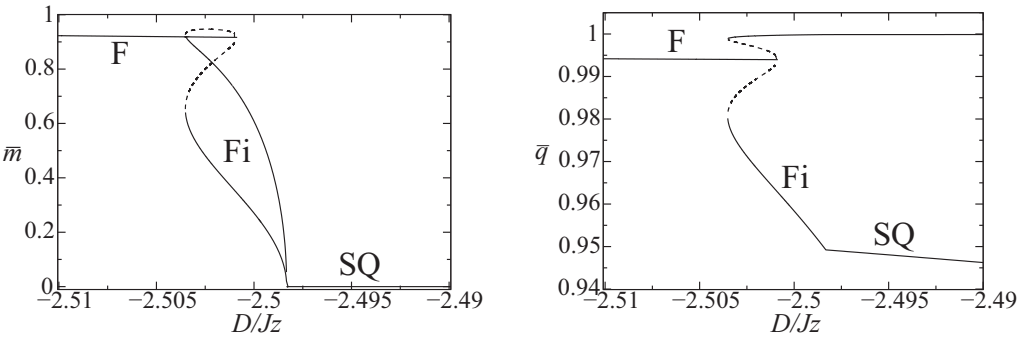

FIG. 3. Bifurcation diagrams of the fixed points $(\bar{m},\bar{q})$ of the auxiliary variables as a function of the parameter D/Jz, with $z = 4$, $K/J = -3.5$, and $t = 0.15$. The dashed lines are associated with an unstable branch of the recurrence relations. Note the costability of two different attractors in the abscissa range $-2.503 \lessapprox D/Jz \lessapprox -2.501$, which coincides with the region of existence of the unstable branch.

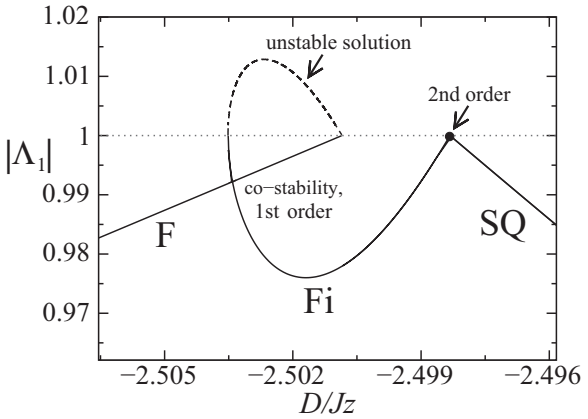

FIG. 4. Absolute value of the largest eigenvalue $|\Lambda_1|$ of the Jacobian matrix as a function of the parameter D/Jz, with $z = 4$, $K/J = -3.5$, and $t = 0.15$. The solid lines represent the numerically stable solutions, while the dashed line represents a numerically unstable branch that indicates the occurrence of a discontinuous (first-order) transition between the coexisting F and Fi phases. Note the costability of both attractors in the abscissa range $-2.503 \lessapprox D/Jz \lessapprox -2.501$. A horizontal dotted line delimits $|\Lambda_1| \leqslant 1$ and the point with $|\Lambda_1| = 1$ denotes a continuous (second-order) transition between the Fi and the SQ phases.

to discuss the thermodynamical stability of the corresponding phases.

IV. BETHE-LATTICE GIBBS FREE-ENERGY DENSITY

In calculations on the BL, the occurrence of a discontinuous (first-order) phase transition is associated with the existence of a range of model parameters (j,k,d,h) in which distinct attractors are dynamically stable under the map application. In other words, different attractors can be reached starting from particular sets of distinct initial conditions for the dynamical map [21,22]. Although the numerical costability of distinct attractors represents a clear indication of occurrence of discontinuous transitions, there are no general rules connecting numerical and thermodynamical stabilities. In order to choose the physical solutions on the BL corresponding to bulk attractors with the lowest Gibbs free energies, a detailed thermodynamic analysis is required. Due to the need to avoid the pathologies originated from the surface sites of a Cayley tree [34–36], the problem is quite delicate and one cannot directly use the Gibbs free energy associated with the entire tree,

$$\begin{aligned}\beta G_N &= -\ln Y_N = -z \ln Q_{N-1}^{(0)} - (z-1) \\ &\quad \times \ln(1 + x_{N-1} + y_{N-1}) \\ &\quad - \ln\left[1 + e^{j+k}\left(x_{N-1}^2 + y_{N-1}^2\right)\right. \\ &\quad \left. + 2(e^{-j+k} x_{N-1}\, y_{N-1} + x_{N-1} + y_{N-1})\right] \\ &= -z(z-1)^{N-1} \ln Q_0^{(0)} + \ln(1 + x_{N-1} + y_{N-1}) \\ &\quad - z \sum_{n=0}^{N-1} (z-1)^{N-1-n} \ln(1 + x_n + y_n) \\ &\quad - \ln\left[1 + e^{j+k}\left(x_{N-1}^2 + y_{N-1}^2\right)\right. \\ &\quad \left. + 2(e^{-j+k} x_{N-1}\, y_{N-1} + x_{N-1} + y_{N-1})\right]. \end{aligned} \tag{26}$$

Given that there is an exponential growth of the total number of sites of a Cayley tree with N generations,

$$N_t(N) = 1 + z \sum_{n=0}^{N-1} (z-1)^{N-1-n} = 1 + z\, \tfrac{(z-1)^N - 1}{z-2}, \tag{27}$$

only the extensive contribution of the complete tree survives for the Gibbs free-energy density per site in the thermodynamic limit $(N \to \infty, N_t \to \infty)$,

$$\begin{aligned}\beta g_{\text{tree}} &\equiv \lim_{N\to\infty} \frac{\beta G_N}{N_t(N)} \\ &= -\left(\frac{z-2}{z-1}\right) \sum_{n=0}^{\infty} (z-1)^{-n} \ln(1 + x_n + y_n), \end{aligned} \tag{28}$$

in disagreement with the free-energy density βf given by Eq. (10) of [22].

Although it would be possible, in principle, to obtain the BL Gibbs free-density density by integration of the equations of state of the order parameters [32,33], Eqs. (18) and (19) and (21)–(24), we resort to a method introduced by Gujrati [31], who proposed to obtain the BL free energy by cleverly subtracting the contribution from the surface sites of the tree. According to Gujrati's method [31], the analytical Gibbs free-energy density per site (in unities of $k_B T$) associated with a

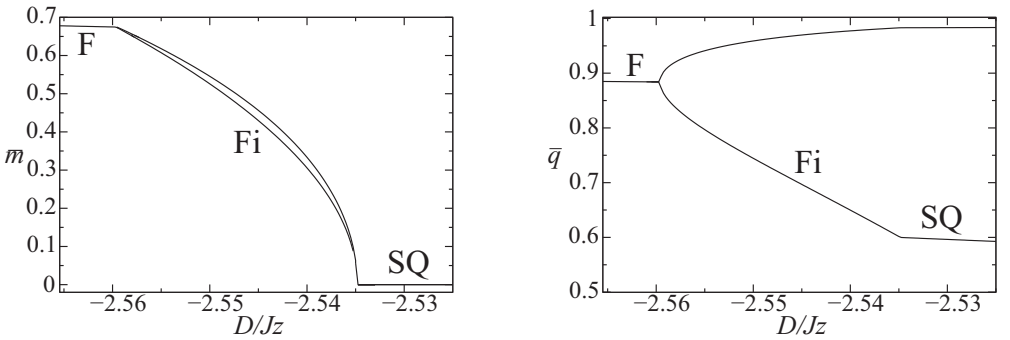

FIG. 5. Bifurcation diagrams of the fixed points $(\bar{m},\bar{q})$ of the auxiliary variables as a function of the parameter D/Jz, with $z = 6$, $K/J = -3.5$, and $t = 0.4$. The phase labels and the meaning of the distinct branches are the same as in Fig. 2.

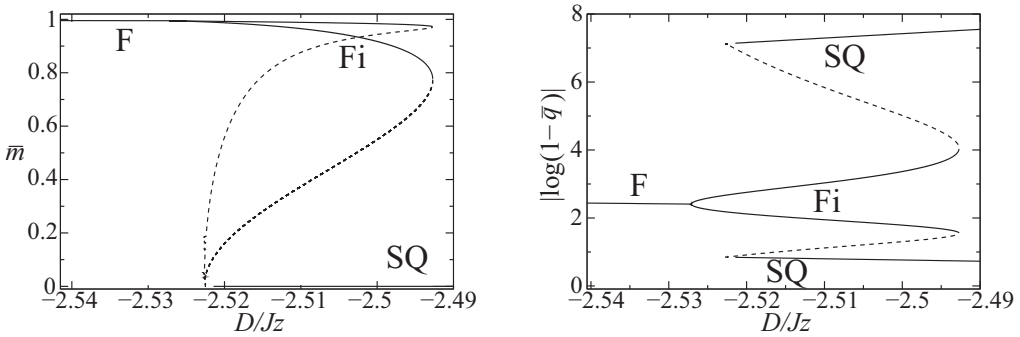

FIG. 6. Bifurcation diagrams of the fixed points $(\bar{m},\bar{q})$ of the auxiliary variables as a function of the parameter D/Jz, with $z=6$, $K/J=-3.5$, and $t=0.1$. The dashed lines are associated with an unstable branch of the recurrence relations. A logarithmic scale for $\bar{q}$ is used for a better visualization of the branches profile, since they are close to $\bar{q}=1$. Note the costability of two different attractors in the abscissa range $-2.523 \lessapprox D/Jz \lessapprox -2.493$, which coincides with the region of existence of the unstable branch.

single fixed point (x,y) reads

$$\begin{aligned}\beta g &= \frac{1}{2}\lim_{N\to\infty}[\beta G_N-(z-1)\beta G_{N-1}]\\ &= -\frac{1}{2}\lim_{N\to\infty}[\ln Y_N-(z-1)\ln Y_{N-1}]\\ &= -(z-1)\ln(1+x+y)+\frac{1}{2}(z-2)\\ &\quad\times\ln[1+e^{j+k}(x^2+y^2)\\ &\quad+2(e^{-j+k}xy+x+y)],\end{aligned}\tag{29}$$

where the thermodynamic limit $N\to\infty$ is taken by evaluating the tree partition functions Y_n at the single fixed point (x,y) of the map, which satisfies Eqs. (10) and (11). One should also remark that Eq. (10) of [22] provides the free-energy density $\beta f=-2\beta g/(z-2)$, although it was claimed that $\beta f=-\frac{1}{N_t(N)}\ln Y_N$, in disagreement with Eq. (28).

The Gibbs free-energy density per site given by Eq. (29) allows one to characterize only the uniform (P and F) phases. However, it is known from previous calculations on the BL [21,22] that, under some conditions, alternate (Fi and SQ) thermodynamic phases arise. In order to be able to characterize these alternate phases, it is necessary to split the system in two interpenetrating sublattices (a,b). The free-energy density per site with the division of the Cayley tree in two sublattices is also obtained using Gujrati's method [31], but now we have to consider Cayley trees with central sites in the two distinct sublattices, leading to

$$\begin{aligned}\beta g &= -\frac{1}{2}\lim_{N\to\infty}\left[\ln Y_N^a-(z-1)\ln Y_{N-1}^b\right]\\ &= -\frac{1}{2}\lim_{N\to\infty}\left[\ln Y_{N+1}^b-(z-1)\ln Y_N^a\right]\\ &= -\frac{1}{2}(z-1)[\ln(1+x_a+y_a)+\ln(1+x_b+y_b)]\\ &\quad+\frac{1}{2}(z-2)\ln[1+e^{j+k}(x_ax_b+y_ay_b)\\ &\quad+e^{-j+k}(x_ay_b+x_by_a)+x_a+x_b+y_a+y_b],\end{aligned}\tag{30}$$

with (x_a,x_b,y_a,y_b) satisfying the coupled system of nonlinear Eqs. (12) and (13), enforcing the thermodynamic limit once the two-cycle fixed point is reached. The Gibbs free-energy density (30) reduces to Eq. (29) by setting $x_a=x_b=x$ and $y_a=y_b=y$, as expected. It is noteworthy that Eq. (30) is invariant by permutation of the sublattice labels (a,b), so that the free-energy densities obtained either with the central site in a, or in b, are exactly the same.

With the free-energy densities of the uniform and the staggered phases, Eqs. (29) and (30), we are then able to locate the discontinuous transitions inside the numerical costability regions. Complementing the previous numerical-stability analysis of Sec. III of the attractors on the BL by the associated Gibbs free-energy densities, Eqs. (29) and (30), allows one to sort out the physically acceptable BL phases and to locate the first-order phase boundaries between them. Recall from

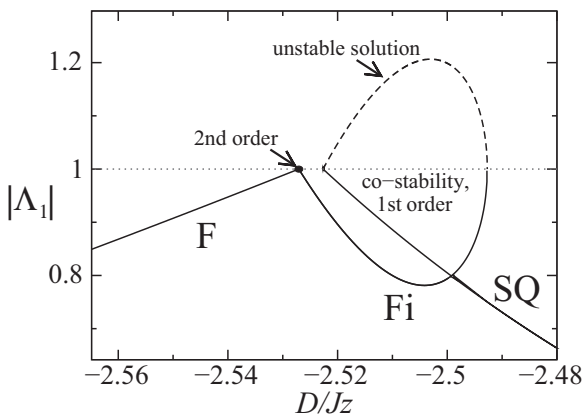

FIG. 7. Absolute value of the largest eigenvalue $|\Lambda_1|$ of the Jacobian matrix as a function of the parameter D/Jz, with $z=6$, $K/J=-3.5$, and $t=0.1$. The solid lines represent the numerically stable solutions, while the dashed line represents a numerically unstable branch that indicates the occurrence of a discontinuous (first-order) transition between the coexisting Fi and SQ phases. Note the costability of both attractors in the abscissa range $-2.523 \lessapprox D/Jz \lessapprox -2.493$. A horizontal dotted line delimits $|\Lambda_1|\leqslant 1$ and the point with $|\Lambda_1|=1$ denotes a continuous (second-order) transition between the F and the Fi phases.

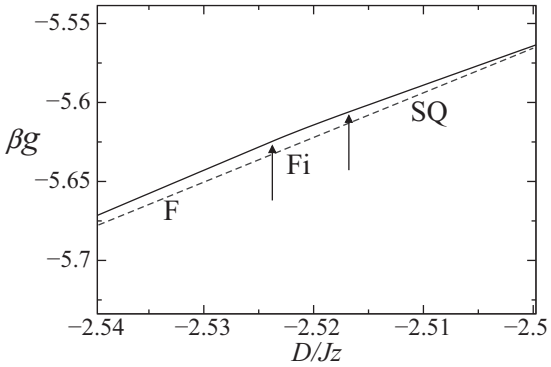

(a) Profile for $z = 4$ and $t = 0.3$.

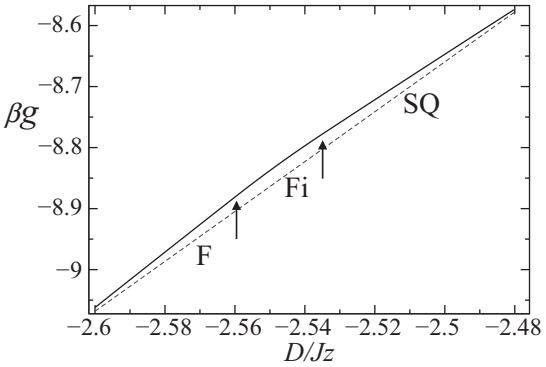

(b) Profile for $z = 6$ and $t = 0.4$.

FIG. 8. Gibbs free-energy profiles (solid lines) associated with the unique numerically stable solutions, obtained for $K/J = -3.5$ and temperatures above the tricritical temperature. The dashed line is only a reference straight line. Only continuous phase transitions (indicated by the arrows) between the different labeled phases are observed, associated with the absence of numerical costability of distinct attractors. These continuous transitions are given by the criterion $|\Lambda_1| = 1$ on the absolute value of the largest eigenvalue of the Jacobian matrix.

Sec. III that, for lower coordinations ($z = 4$), we have found numerical costability between attractors associated with the F and Fi phases, while for higher coordinations ($z = 6$), the numerical costability takes place between attractors associated with the Fi and the SQ phases. We expect, therefore, a character change of the phase transitions between the given different phases, depending on the lattice coordination z. By combining results from Secs. III and IV, we can obtain free-energy profiles of the BL solutions. Figures 8 and 9 display, respectively, cases where continuous and discontinuous transitions were detected.

Figure 8 displays cases that do not present numerical costability of different attractors. The chosen parameters for Fig. 8 coincide with those used to plot Figs. 2 and 5. Therefore, the observed phase transitions are always continuous, associated with bifurcations of the fixed points. Due to the fact that the Gibbs free-energy derivatives calculated at a continuous transition are the same for the two involved phases, it is difficult to observe a change of behavior of the free-energy branches shown in Fig. 8. A dashed line of reference and arrows indicating the continuous transitions are added to the free-energy profile in order to improve the visualization of the phase transitions.

On the other hand, Fig. 9 displays cases that do present numerical costability of different attractors, indicating that the observed phase transitions are discontinuous. The chosen parameters for Fig. 9 coincide with those used to plot Figs. 3 and 6, and also Figs. 4 and 7 for $|\Lambda_1|$. In Fig. 9(a) it is possible to note that the free energies of the two coexisting phases intersect near the abscissa -2.5028, while in Fig. 9(b) the intersection occurs near the abscissa -2.5. These intersections locate the discontinuous (first-order) phase transitions.

V. GLOBAL $T \times D$ PHASE DIAGRAMS

By collecting the location of the phase transitions (continuous and discontinuous), as well as the costability regions of distinct attractors, it is possible to draw the global $t \times D/Jz$ phase diagrams of the ferromagnetic BEG model with repulsive biquadratic interactions ($K/J = -3.5$) and vanishing external magnetic field ($H = 0$) obtained on the BL for the two investigated coordinations, $z = 4$ and $z = 6$, shown respectively in Figs. 10 and 11. The multicritical behavior of

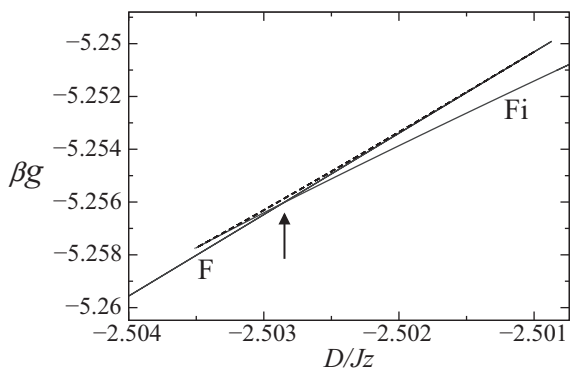

(a) Profile for $z = 4$ and $t = 0.15$.

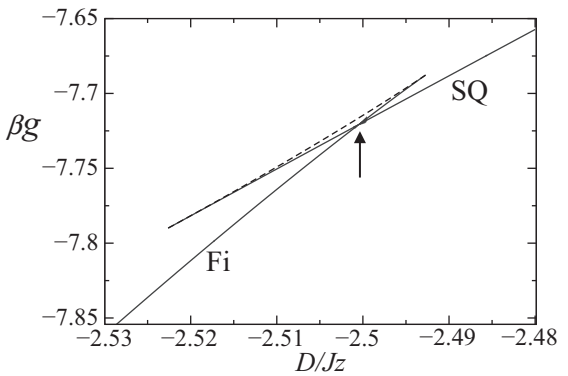

(b) Profile for $z = 6$ and $t = 0.1$.

FIG. 9. Gibbs free-energy profiles associated with the numerically stable (solid lines) and unstable (dashed lines) solutions, obtained for $K/J = -3.5$ and temperatures below the tricritical temperature. The numerical costability of two distinct attractors indicates the occurrence of a discontinuous (first-order) phase transition between the two coexisting labeled phases. The point where the Gibbs free energies of the stable branches intersect (indicated by the arrows) locates the discontinuous phase transition.

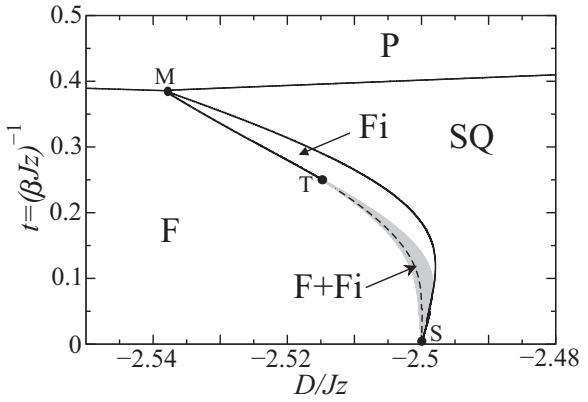

FIG. 10. Global phase diagram of the ferromagnetic BEG model with repulsive biquadratic interations ($K/J = -3.5$) on a BL with coordination $z = 4$. The numerical costability region is shaded in gray. The dashed line represents the discontinuous (first-order) phase boundary, while the solid lines correspond to continuous (second-order) transitions. The labels of the thermodynamic phases (P, F, Fi, SQ) and the classification of the special points (M, T, S) follow the main text.

both typical phase diagrams is very rich, displaying several special points:

(i) a tetracritical point (M), where four second-order lines separating the P/F, P/SQ, Fi/F, and Fi/SQ phases meet;

(ii) a tricritical point (T), where a low-temperature first-order line turns into a high-temperature second-order line;

(iii) a highly degenerate zero-temperature point (S), where a second-order line and a first-order line meet at zero temperature.

Table I summarizes the representative features of the two distinct typical phase diagrams. In particular, the type of the transitions with the Fi phase changes with the coordination z. For low coordinations ($z = 4$), the Fi/SQ transition is always continuous, whereas for high coordinations ($z = 6$), the transition that is always continuous corresponds to the Fi/F transition. There is a tricritical point T along the Fi/F transition for lower coordinations ($z = 4$), while it occurs on

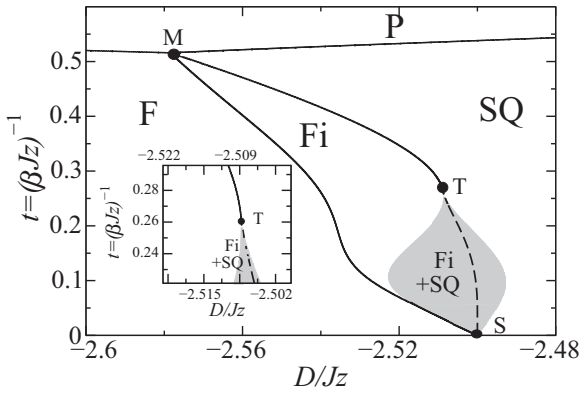

FIG. 11. Global phase diagram of the ferromagnetic BEG model with repulsive biquadratic interations ($K/J = -3.5$) on a BL with coordination $z = 6$. The numerical costability region is shaded in gray. The dashed line represents the discontinuous (first-order) phase boundary, while the solid lines correspond to continuous (second-order) transitions. The labels are the same as those used in Fig. 10.

TABLE I. Type of the phase transitions for the ferromagnetic BEG model with repulsive biquadratic interactions ($K/J = -3.5$) and vanishing external magnetic field ($H = 0$) obtained on the BL with coordination z. Most of the transitions are continuous, but a few switch order at a tricritical temperature T_T.

Phase transition	Low coordination ($z = 4$)	High coordination ($z = 6$)
P/F	continuous	continuous
P/SQ	continuous	continuous
Fi/SQ	continuous	continuous for $T \geqslant T_T$ discontinuous for $T < T_T$
Fi/F	continuous for $T \geqslant T_T$ discontinuous for $T < T_T$	continuous

the Fi/SQ transition for higher coordinations ($z = 6$). However, all transitions with the high-temperature disordered P phase are continuous, independently of the coordination z. The picture found for higher coordinations ($z = 6$) is consistent with previous results obtained in the MFA [12–14].

VI. CONCLUDING REMARKS

We present an exact solution of the spin-1 BEG model on a Cayley tree, formulated in terms of a set of nonlinear discrete recursion relations, whose attractors correspond to physically acceptable solutions on the BL in the deep interior of the Cayley tree [32,33]. The presence of overlapping regions, where distinct attractors are numerically costable, represents a clear indication of occurrence of discontinuous (first-order) phase transitions. We then resort to Gujrati's method [31] to write analytical closed expressions of a *bona fide* Gibbs free-energy density on the BL, both for the cases of the uniform (P and F), as well as for the staggered (Fi and SQ) thermodynamic phases. The thermodynamic consistency of the obtained free energy can be checked by the recovery of the BPA equations of state for the BL order parameters. By analyzing the numerical stability of the map attractors and comparing their associated Gibbs free energies, we are then able to locate the first-order phase boundaries and draw global phase diagrams in terms of the temperature T and crystal field D, for two different typical lattice coordinations, $z = 4$ and $z = 6$.

We found that, for the ferromagnetic version ($J > 0$) with the inclusion of crystal fields ($D \neq 0$) in the regime of repulsive biquadratic interactions ($K/J = -3.5$) and vanishing external magnetic fields ($H = 0$), there is a change of the type of the Fi/F and Fi/SQ transitions, depending on the coordination z of the BL. The presence of a tricritical point is also coordination dependent: for lower coordinations ($z = 4$), it occurs on the Fi/F boundary, while for higher coordinations ($z = 6$), it takes place on the Fi/SQ transition. It should be remarked that, in two dimensions, even the existence of the narrow Fi phase squeezed between the F and the SQ phases is not supported by RG [12,24,25] and MCSs [25,29]. However, the existence of a tricritical point along the F/SQ boundary is less clear in the MCS for the square lattice, as can be seen in Fig. 5 of Ref. [25].

Although the high-coordination ($z = 6$) results are consistent with previous MFA calculations [12–14], which can be formally obtained for a BL in the infinite-coordination

limit ($z \to \infty$), it remains an open question whether they are robust against dimensionality changes. RG calculations [12,24,25] predict, for example, that the Fi phase is present in three dimensions, but not in two dimensions. Because BL calculations rely on a pair approximation, they cannot distinguish a three-dimensional cubic lattice from a two-dimensional triangular lattice, since both share the same coordination $z = 6$.

ACKNOWLEDGMENTS

We acknowledge financial support from the Brazilian agencies CNPq (Conselho Nacional de Desenvolvimento Científico e Tecnológico) [Grant No. 132988/2014-3] and CAPES (Coordenação de Aperfeiçoamento de Pessoal de Nível Superior) [Grant No. 1583164].

[1] E. Ising, Z. Phys. **31**, 253 (1925).
[2] M. Blume, V. J. Emery, and R. B. Griffiths, Phys. Rev. A **4**, 1071 (1971).
[3] J. Lajzerowicz and J. Sivardière, Phys. Rev. A **11**, 2079 (1975).
[4] J. Sivardière and J. Lajzerowicz, Phys. Rev. A **11**, 2090 (1975).
[5] D. Mukamel and M. Blume, Phys. Rev. A **10**, 610 (1974).
[6] J. Sivardière and J. Lajzerowicz, Phys. Rev. A **11**, 2101 (1975).
[7] D. Furman, S. Dattagupta, and R. B. Griffiths, Phys. Rev. B **15**, 441 (1977).
[8] K. E. Newman and J. D. Dow, Phys. Rev. B **27**, 7495 (1983).
[9] M. Schick and W.-H. Shih, Phys. Rev. B **34**, 1797 (1986).
[10] H. S. Guidi and V. B. Henriques, Phys. Rev. E **90**, 052705 (2014).
[11] M. A. A. Barbosa and V. B. Henriques, Phys. Rev. E **77**, 051204 (2008).
[12] W. Hoston and A. N. Berker, J. Appl. Phys. **70**, 6101 (1991).
[13] W. Hoston and A. N. Berker, Phys. Rev. Lett. **67**, 1027 (1991).
[14] C. Ekiz and M. Keskin, Phys. Rev. B **66**, 054105 (2002).
[15] A. Erdinç, O. Canko, and M. Keskin, J. Magn. Magn. Mater. **301**, 6 (2006).
[16] K. G. Chakraborty and T. Morita, Physica A **129**, 415 (1985).
[17] M. J. de Oliveira and S. R. Salinas, Braz. J. Phys. **15**, 189 (1985).
[18] R. Osório, M. J. de Oliveira, and S. R. Salinas, J. Phys.: Condens. Matter **1**, 6887 (1989).
[19] K. Kasono and I. Ono, J. Magn. Magn. Mater. **104–107**, 282 (1992).
[20] K. Kasono and I. Ono, Z. Phys. B: Condensed Matter **88**, 205 (1992).
[21] M. N. Tamashiro and S. R. A. Salinas, Physica A **211**, 124 (1994).
[22] A. Z. Akheyan and N. S. Ananikian, J. Phys. A: Math. Gen. **29**, 721 (1996).
[23] A. N. Berker and M. Wortis, Phys. Rev. B **14**, 4946 (1976).
[24] R. R. Netz and A. N. Berker, Phys. Rev. B **47**, 15019 (1993).
[25] N. S. Branco, Physica A **232**, 477 (1996).
[26] R. R. Netz, Europhys. Lett. **17**, 373 (1992).
[27] A. Rosengren and S. Lapinskas, Phys. Rev. Lett. **71**, 165 (1993).
[28] Y. Wang and C. Wentworth, J. Appl. Phys. **61**, 4411 (1987).
[29] Y.-L. Wang, F. Lee, and J. D. Kimel, Phys. Rev. B **36**, 8945 (1987).
[30] A. Rachadi and A. Benyoussef, Phys. Rev. B **69**, 064423 (2004).
[31] P. D. Gujrati, Phys. Rev. Lett. **74**, 809 (1995).
[32] C. J. Thompson, J. Stat. Phys. **27**, 441 (1982).
[33] R. J. Baxter, *Exactly Solved Models in Statistical Mechanics, 3rd printing*, Dover Books on Physics Series (Dover, Mineola, NY, 2007), Chap. 4, pp. 47–59.
[34] L. K. Runnels, J. Math. Phys. **8**, 2081 (1967).
[35] T. P. Eggarter, Phys. Rev. B **9**, 2989 (1974).
[36] E. Müller-Hartmann and J. Zittartz, Phys. Rev. Lett. **33**, 893 (1974).
[37] K. Huang, *Statistical Mechanics*, 2nd ed. (Wiley, New York, 1987), Sec. 14.5, pp. 357–361.
[38] R. K. Pathria, *Statistical Mechanics*, 2nd ed. (Butterworth-Heinemann, Oxford, 1996), Sec. 11.6, pp. 328–334.
[39] D. A. Lavis and G. M. Bell, *Closed-form and Exact Solutions*, Statistical Mechanics of Lattice Systems Vol. 1 (Springer-Verlag, Berlin, 1999), Sec. 7.3, pp. 178–181.
[40] S. R. A. Salinas, *Introduction to Statistical Physics* (Springer-Verlag, New York, 2001), Sec. 13.4, pp. 268–271.
[41] J. Guckenheimer and P. Holmes, *Nonlinear Oscillations, Dynamical Systems, and Bifurcations of Vector Fields* (Springer-Verlag, New York, 1983), Sec. 1.4, pp. 16–22.